Balloon measurements of the vertical ionization profile over southern Israel and comparison to mid-latitude observations

Roy Yaniv[1], Yoav Yair[2], Colin Price[1], Keri Nicol[3], Giles Harrison[3], Anton Artamonov[4] and Ilya Usoskin[4]

[1] Department of Geosciences, Tel-Aviv University, Tel-Aviv, Israel.

[2] School of Sustainability, Interdisciplinary Center (IDC) Herzliya, Israel

[3] Department of Meteorology, University of Reading, United Kingdom.

[4] Space Climate group, Faculty of Science, University of Oulu, Finland.

Abstract

Airborne measurements using meteorological balloons were conducted for the first time from southern Israel (geographic $30^{o}35$'N, $34^{o}45$'E geomagnetic $27^{o}6$'N $112^{o}23$'E) for measuring the vertical ionization profile during solar cycle 24. The results show the differences (increase of ~30%) in count rates as we proceed from solar maximum toward solar minimum. The observed altitude of maximum ionization (the Regener-Pfotzer maximum) was between 17-20 km, and it agrees well with results from other simultaneous measurements conducted at different latitudes (Reading, UK and Zaragoza-Barcelona, Spain). When compared with predictions of an analytical model, we find a highly significant correlation (R^2=0.97) between our observations and the computed ionization profiles. The difference in count rates can be attributed to the height of the tropopause due to the model using a US standard atmosphere that differs from the measured atmospheric parameters above Israel.

1. Introduction

Over land and within the boundary layer (few hundred meters) the atmosphere is mostly ionized by radiation emitted from the decay of radioactive isotopes in the Earth's crust. Hess [1912] studied the ionization profile in the atmosphere and postulated that ionization should therefore decrease with altitude since the radioactive elements have a source near the surface. However, using balloon measurements Hess found that ionization increased at altitudes above 10 km, and interpreted the results as caused by an external source, namely galactic cosmic rays (GCR). He claimed that the penetration depth of these particles was dependent on the energy spectrum of the incoming radiation [Hess 1912]. Regener extended Hess' measurements using balloons, reaching heights up to 20km (Regener 1933). They found that the ionization from cosmic rays reaches its maximum value at altitudes between 17-24 km and is known as the Regener-Pfotzer maximum (RP max) and is geomagnetic-latitude dependent (Pfotzer 1936, Carlson and Watson 2014). Figure 1 shows past and present measurements of the ionization profile (counts/sec/cm^2/steradian) from a V-2 rocket up to 80 km at 40° geomagnetic latitude,

59   and a sounding balloon launch up to 30km from Reading, UK with a ionization model fit

60   overlaid. In both locations the RP max can be clearly observed [Israël 1970; Harrison et

61   al., 2014].

62   Up to 40 km above the surface the main ionization source in the atmosphere is

63   GCR and, sporadically in the polar region, solar protons [Mironova et al., 2015]. Balloon

64   measurements of charged particle fluxes (> 1MeV) and ion production rates have been

65   performed continuously from 1957 by the Lebedev Physics Institute, Russia

66   [Bazilevskaya et al 2000, Bazilevskaya et al 2008]. They found a correlation between the

67   ratio of ion production rate (q) and the cosmic charged particle flux (J) during days with

68   no solar activity at polar latitudes given by: $\frac{q}{J} = Ae^{-BH}$ (where A= 119.86 cm−1 ; B =

69   0.148, and H is the altitude [km] − Bazilevskaya et al 2000 their Figure 4). The flux of

70   cosmic rays reaching the atmosphere at any given location is a function of the energy

71   spectrum, which is also impacted by solar activity, on short and long temporal scales and

72   by the geomagnetic rigidity cutoff, effectively determined by the geomagnetic latitude.

73   The rigidity is a key parameter for particle motion in magnetic fields and is defined as the

74   particle's momentum over charge: particles cannot penetrate to locations where the

75   geomagnetic cutoff is greater than the particle's rigidity (Bazilevskaya 2005, Smart et al

76   2006, Mironova et al., 2015).

77   Simultaneous ground and airborne measurements using a balloon equipped with

78   an ionization counter (based on a Geiger tube) have previously been performed during

79   quiet atmospheric conditions and during a solar flare event from Reading, UK [Nicoll and

80   Harrison, 2014; Harrison et al., 2014]. During the solar flare, the X-ray burst was

81   followed by a solar proton event that caused changes in the atmospheric electrical

82   properties of the potential gradient and the conduction current at ground level, with an

83   observed increase of more than 20% in the ionization at 20km, deduced from the RP max

84   values that were measured relative to quiet conditions.

85

86   **2. Methodology**

2.1 Instrumentation

Measurements of the atmospheric ionization up to the height of 35 km were conducted using standard radiosonde balloons equipped with additional disposable ionization sensors developed by the University of Reading. The ionization sensor is composed of two LND714 miniature Geiger tubes which uses a microcontroller to count the number of ionization events (the impact of a gamma photon counts as one event) that occur within each tube per minute interval [Harrison et al., 2013]. Count rates reported here are the mean count rate from both tubes. Each Geiger tube was calibrated by the manufacturer using a Co-60 Ionization source with a gamma sensitivity of 1.5 (counts s^{-1})/(mR hour^{-1}) (Harrison et al., 2012; Harrison et al., 2013). The ionization sensor is interfaced to a standard Vaisala RS92 radiosonde via the PANDORA data acquisition system (Harrison et al, 2012).

The balloons were launched from the Wise Observatory in Mitzpe Ramon (30^o35'N, 34^o45'E, altitude 850 m a.s.l.). This location is in an arid region of the southern part of Israel (the Negev highland desert) remote from Israel's major cities and other sources of pollution. The area's climate typically exhibits hot and dry summers with average daily temperature of 30 $^{\circ}$C and cold winters with average temperature of 6 $^{\circ}$C. These conditions readily facilitate other atmospheric electrical measurements (vertical E-field, vertical conduction current, ELF and VLF), as described in Price and Melnikov (2004), Elhalel et al. (2014) and Yaniv et al. (2016). We note that these are the first such measurements ever conducted in Israel, and for that matter, in this low geomagnetic latitude range. Thus, the measurements offer a much needed addition to the global map of cosmic ray ionization, which is traditionally based on balloon measurements conducted at mid and high-latitudes.

2.2 Model Description

We used the CRAC:CRII model of atmospheric ionization [Usoskin and Kovaltsov, 2006; Usoskin et al., 2010], based on Monte Carlo calculations which simulate the ionization by cosmic rays (interactions of particles (protons, alpha-particles

116 and heavy species) and locally produced secondary particles (protons, electrons,
117 neutrons and muons)), enabling a comparison between observations and theoretical
118 predictions. The model output provides the vertical profile of the ion production rate and
119 is applicable to a US standard atmosphere. The predictions of the model have been
120 validated over a wide range of geographical latitudes and altitudes [Usoskin and
121 Kovaltsov 2006; Harrison et al 2014]. The model can assess the ionization rate by cosmic
122 rays, by considering the geomagnetic rigidity cutoff at the site and the actual cosmic ray
123 intensity as monitored by ground-based neutron monitors.

124   Atmospheric ionization is mostly defined by the flux of GCR outside the
125 atmosphere, which is modulated by solar activity: the GCR flux is greater for low solar
126 activity periods and visa versa. Solar modulation of GCR is often quantified via the
127 modulation potential [Usoskin et al., 2005]. Values of the modulation potential for the
128 days of the reported balloon flights are given in Table 1. One can see that the modulation
129 potential decreased in time between the launches, reflecting the declining phase of solar
130 activity in the present solar cycle.

131

132 **3. Results**

133   Six balloon launches were conducted during the period from October 2014 to June
134 2016 reaching altitudes of ~18, 29, 28, 34, 35 and 28km. Starting with launch #3 we also
135 used a parachute to measure parameters during descent. Table 1 summarizes the
136 operational aspects of our airborne campaign including flight duration, peak pressure at
137 the highest altitude, lowest temperature measured during the flight and the highest count
138 rate representing the RP max altitude. Figure 2 shows the flight trajectories on a regional
139 map, indicating that some balloons drifted with the stratospheric winds to Jordan and
140 Egypt, and were thus not retrievable.

141   Figures 3a, 3b and 3c present the vertical profiles of the temperature, pressure and
142 relative humidity respectively showing the meteorological conditions for each launch.
143 Figures 3a and 3b also show temperature and pressure from the U.S. Standard

144 Atmosphere 1976, (NASA-TM-X-74335), which agree well with the sounding profiles,

145 although some differences can be clearly noted, as we will discuss later on.

146   Figure 4a shows the count rates of the Geiger counters as a function of altitude for

147 each launch and the mean calculated ionization curve (black line) which peaks in the

148 height range of 17-20 km. According to the 1976 US standard atmosphere values

149 (http://www.digitaldutch.com/atmoscalc/), the height range of 17-20 km measured in the

150 mean ionization curve corresponds to the pressure of 100 mbar as shown in Fig. 4b.

151 Figure 4b is a fit of the count rate versus the measured atmospheric pressure and is in

152 agreement with Fig. 1b. Figure 4b shows that from 2014 to 2016 the ionization value had

153 steadily increased by ~30%.

154   Bazilevskaya (2014) noted an impact of the solar cycle on the flux of GCR

155 arriving to Earth's atmosphere. Maximum solar activity diminishes the flux of GCR

156 while minimum activity increases the flux of GCR. Figure 5 shows the negative linear

157 correlation between the RP max counts per minute and the modulation potential. Flight

158 #4 (27 Aug 2015) was conducted during an M class solar flare event with Kp=7 while

159 flight #5 was conducted in fair weather on a quiet solar day.

160   The second launch was conducted simultaneously with other launches at various

161 locations in order to compare the vertical ionization profiles at different geomagnetic

162 latitudes during 22nd -24th October 2014 (Makhmutov et al., 2015). Figure 6 shows the

163 fit of the ionization profile as was measured by ionization sensors from Mitzpe Ramon

164 (Israel), Zaragoza-Barcelona (Spain) and Reading (UK). We can clearly see the

165 differences in the RP maximum altitude and the count rate as a function of the

166 geomagnetic latitudes. The Reading flight shows a higher count rate, followed by

167 Zaragoza-Barcelona measurement while the Israeli flight shows the lowest count rate.

168 Figure 7 presents the CRAC:CRII model results of the ion production rate as a function

169 of height for the Israel-Spain-UK balloon flights. We used the model to simulate the

170 ionization rate in the atmosphere as a function of the geomagnetic latitudes for the

171 simultaneous launches conducted from Israel, Spain and the UK during 22-24 Oct 2014.

172 Harrison et al., (2014) used a factor of 2.95 for a standard atmosphere to convert the

173   ionization count rates (in counts min^{-1}) to ion production rates. Using this conversion

174   coefficient we found a good correlations (R^2>0.9) between the actual measurement from

175   Israel and the model from the 22 Oct 2014 (Figure 8 top) and the 14 May 2015 launch

176   (Figure8 bottom).

177

178   4. Discussion

179   We present results of airborne measurement conducted for the first time above

180   Israel and from a low latitude location, adding new information on the latitudinal

181   dependence of cosmic ray induced ionization, and complementing the majority of

182   airborne measurements that were performed at mid and high latitudes over Europe,

183   Russia and the US.

184   The difference (10-35% lower) in the meteorological parameters shown in figure

185   3a and 3b compared with the U.S standard atmosphere model is especially pronounced in

186   the temperature profile near the tropopause. As discussed below, this US Standard

187   Atmosphere, when used in the CRAC:CRII model, is the main reason for differences

188   between our observations and the model results. Figure 3c also shows large variability in

189   the vertical profile of the relative humidity, indicating periods when the balloon ascended

190   through layers of visible clouds. We visually observed and identified the relevant cloud

191   types, as indicted in the graphs.

192   4.1 Solar activity impact on ionization:

193   The ionization increase shown in Figure 4a and Figure 4b results from the overall

194   increase of the GCR flux impacting the Earth due to a decrease in the activity of the sun –

195   reflecting the declining phase of solar cycle 24. Table 1 shows values of the modulation

196   potential (cosmic ray modulation parameter deduced from the sunspot index (Nymmik et

197   al., 1996). It is clearly evident from Figure 5 that ionization count rates increase from ~30

198   cpm to ~50 cpm as the modulation potential decreases, as more GCR penetrate into the

199   Earth's atmosphere indicating that the sun is approaching solar minimum. During a solar

200   event that occurred during the launch of 27 Aug 2015 (Kp 7), we observed no impact on

201   the ionization profile, likely because of the high cutoff rigidity at the latitude of Israel.

202 We can conclude that short term variations are too small to be recorded using our
203 instrument, but long term variations in solar activity can be monitored. Similar results
204 were found by Harrison (2014) during the rising phase of solar cycle 24 toward solar
205 maximum with ionization values of the RP max decreasing from around 80 cpm in 2013
206 to 60 cpm in 2014.

207   4.2 Geomagnetic latitude effect on ionization:

208   The differences found between the ionization values from Israel, Spain and the
209 UK shown in Figure 6 are due to geomagnetic shielding (stronger deflection of charged
210 GCR particles by the magnetosphere at the lower latitude of Israel). While high and mid-
211 latitude measurements of the vertical ionization profile are quite abundant [Nicoll 2012],
212 results in low-latitudes and sub-tropical regions are quite rare, and none have been
213 reported in the geomagnetic latitude of Israel (~27N) where the cutoff rigidity is 10.3GV
214 (compared to Spain 4.6GV and the UK 3.6GV). It is observable that the altitude of the
215 RP max at all locations is in good agreement while the intensity of the GCR penetrating
216 decrease as we proceed from polar to equatorial latitudes – values ranged around 25, 40
217 and 50 cpm for Israel, Spain and UK respectively. Measurements in polar latitudes
218 (Mirny, Antarctica (geomagnetic latitude 67.23 S) with cutoff rigidity of 0.03 GV and
219 Apatity, Russia (geomagnetic latitude 68.14 N) with cutoff rigidity of 0.56 GV) obtained
220 by Makhmutuv et al (2014) on the same day but with a different instrument found higher
221 ionization values than the UK.

222   The model results shown in Figure 7 agree well with the simultaneous
223 measurements showing that ion production rates (ion pairs/cm^3/s) are larger at higher
224 latitudes where the cutoff rigidity is smaller and lower at lower latitudes where the cutoff
225 rigidity is greater, thus, confirming the results presented in Figure 6. Model results for
226 other balloon flights were in good agreement as well while the small differences are
227 likely due to the use of the Standard US atmosphere in the model rather than the actual
228 atmospheric density profiles from the balloon measurements.

229

5. Summary

Balloon measurements of the vertical ionization profile have been conducted for the first time in Israel. We found that the Regener-Pfotzer maximum to be in the expected altitude range of 17-20 km at an atmospheric pressure of ~100 mbar. The effect of the present phase of solar cycle 24 is clearly evident in the measured ionization count rates showing an increase in ionization due to increases in GCR fluxes as expected from the declining phase toward the next solar minimum. Simultaneous measurements from different latitudes using the same Geiger counters found a latitudinal dependence of the count rates as expected – higher count rates (~50 cpm) for the mid-latitudes of Spain and UK where the geomagnetic rigidity is lower compared to the low latitude of Israel (~25 cpm). Model calculations of ion pair-production rate profile were found to correlate positively ($R^2 > 0.9$) with the measurements.

References:

Bartlett, D.T., Tommasino, L., Beck, P., Wissmann, F., O'Sullivan D., Bottollier-Depois, J.-F. and Lindborg L. Investigation of Radiation Doses at Aircraft Altitudes during a Complete Solar Cycle: DOSMAX- A collaborative Research Program. Presented at the 12th Biennial Topical Meeting at XXX 2002.

Bazilevskaya G.A., Krainev M.B., Makhmutov V.S., Effects of cosmic rays on the earth's environment, J. Atmos. Sol.-Terr. Phys. 62, 1577–1586, 2000.

258 Bazilevskaya G.A., Solar cosmic rays in the near Earth space and the atmosphere. Adv.
259   Space Res. 35, 458–464, 2005.

260 Bazilevskaya G.A., Usoskin I.G., Flückiger E.O., Harrison R.G., Desorgher L., Bütikofer
261   R., Krainev M.B., Makhmutov V.S., Stozhkov Y.I., Svirzhevskaya A.K., Svirzhevsky
262   N.S., Kovaltsov G.A., Cosmic ray induced ion production in the atmosphere. Space
263   Sci. Rev. 137, 149–173, 2008.

264 Bazilevskaya, G. A., Cliver, E. W., Kovaltsov, G. A., Ling, A. G., Shea, M. A., Smart, D.
265   F., & Usoskin, I. G., Solar cycle in the heliosphere and cosmic rays. Space Science
266   Reviews, 186(1-4), 409-435, 2014.

267 Carlson, P., & Watson, A. A. (2014). Erich Regener and the ionization maximum of the
268   atmosphere. History of Geo-and Space Sciences, 5(2), 175.

269 Elhalel G., Yair Y., Nicoll K., Price C., Reuveni Y., and Harrison R. G., Influence of
270   short-term solar disturbances on the fair weather conduction current, J. Space Weather
271   Space Clim. 4, A26 DOI: 10.1051, 2014.

272 Friedberg, W., Copeland, K., Duke, F. E., O'Brien III, K., & Darden Jr, E. B. Guidelines
273   and technical information provided by the US Federal Aviation Administration to
274   promote radiation safety for air carrier crew members. Radiation Protection
275   Dosimetry, 86(4), 323-327, 1999.

276 Harrison, R. G., Nicoll, K. A., Lomas A. G., Programmable data acquisition system for
277   research measurements from meteorological radiosondes, Rev. Sci. Instrum., 83,
278   036106, 2012.

279 Harrison, R. G., Nicoll, K. A., Lomas A. G., Geiger tube coincidence counter for lower
280   atmosphere radiosonde measurements, Rev. Sci. Instrum., 84, 076103, 2013.

281 Harrison, R. G., Nicoll, K. A., Aplin, K. L., Vertical profile measurements of lower
282   troposphere ionization. Journal of Atmospheric and Solar-Terrestrial Physics, 119,
283   203-210., 2014.

284 Hess V. F., Über beobachtungen der durchdringenden Strahlung bei sieben
285   Freiballonfahrten, Zeitschrift fur Physik, vol. 13, pp. 1084–1091, 1912.

286   Israël, H. Atmospheric electricity: Atmosphärische Elektrizität. Vol. 29. Israel Program
287   for Scientific Translations [available from the US Dept. of Commerce, National
288   Technical Information Service, Springfield, Va.(Jerusalem), 1970.

289   Makhmutov, V., Bazilevskaya, G., Stozhkov, Y., Philippov, M., Yair, Y., Yaniv, R.,
290   Harrison G., Nicoll K. and Aplin, K. Cosmic ray measurements in the atmosphere at
291   several latitudes in October, 2014, Proceeding of Science, ICRC 2015.

292   Mishev, Alexander, and Ilya Usoskin, Numerical model for computation of effective and
293   ambient dose equivalent at flight altitudes-Application for dose assessment during
294   GLEs, Journal of Space Weather and Space Climate 5, 2015.

295   Mironova, I. A., Aplin, K. L., Arnold, F., Bazilevskaya, G. A., Harrison, R. G.,
296   Krivolutsky, A. A., Nicoll K. A., Rozanov E. V., Turunen E. & Usoskin, I. G.,
297   Energetic Particle Influence on the Earth's Atmosphere. Space Science
298   Reviews, 194(1-4), 1-96, 2015.

299   Nicoll, K. A. "Measurements of atmospheric electricity aloft." Surveys in
300   geophysics 33.5, 991-1057, 2012.

301   Nicoll, K. A., Harrison, R. G., Detection of lower tropospheric responses to solar
302   energetic particles at midlatitudes. Physical review letters, 112(22), 225001, 2014.

303   Nymmik R.A., Panasyuk M.I. et Suslov A.A., Adv. Space Research, 17, (2)19-(2)30,
304   1996.

305   Pfotzer, G., Dreifachkoinzidenzen der Ultrastrahlung aus vertikaler Richtung in der
306   Stratosphare, II, Analyse der gemessenen Kurve, Z. Phys., 102, 41–58, 1936b.

307   Price, C., and A. Melnikov, Diurnal, Seasonal and Inter-annual Variations in the
308   Schumann Resonance Parameters, Journal of Atmospheric and Solar-Terrestrial
309   Physics, 66, 1179-1185, 2004.

310   Regener, E.: New Results in Cosmic Ray Measurements, Nature, 132, 696–698, 1933.

311   Smart, D.F., M.A. Shea, A.J. Tylka, P.R. Boberg, A geomagnetic cutoff rigidity
312   interpolation tool: Accuracy verification and application to space weather. Adv. Space
313   Res. 37, 1206–1217, 2006.

314   Usoskin, I.G., K. Alanko-Huotari, G.A. Kovaltsov, K. Mursula, Heliospheric modulation

315   of cosmic rays: Monthly reconstruction for 1951-2004, J. Geophys. Res., 110(A12),

316   CiteID A12108, 2005.

317   Usoskin I., Kovaltsov G., Cosmic ray induced ionization in the atmosphere: Full

318   modeling and practical applications, Journal of geophysical research 11, D21206,

319   2006.

320   Usoskin, I. G., G. A. Kovaltsov, and I. A. Mironova, Cosmic ray induced ionization

321   model CRAC:CRII: An extension to the upper atmosphere, J. Geophys. Res., 115,

322   D10302, 2010.

323   Yaniv, R., Yair, Y., Price, C., & Katz, S., Local and global impacts on the fair-weather

324   electric field in Israel. Atmospheric Research, Vol 172-173, p. 119-125, 2016.

325

326

327   **Figure Captions:**

328   **Figure 1.** Ionization-altitude curves of ionization from cosmic radiation. (left) past rocket launch [adapted

329   from Israël 1970 his figure 26] and (right) modern balloon launch. [adapted from Harrison et al 2014]

330

331   **Figure 2.** Regional map of Israel and surrounding countries with flight trajectories for each launch.

332

333   **Figure 3.** Vertical temperature profile (a), pressure profile (b) and relative humidity profile (c) for each

334   launch. We note the locations of several cloud types, based on the RH values and visual observations.

335

336   **Figure 4.** Ionization variation versus the altitude [km] (a) and Vertical Ionization profile [counts mins^{-1},

337   cpm] versus the Pressure [mbar] (b). The black line shows the average value of 6 launches

338

339   **Figure 5.** Modulation potential as a function of the Ionization count rate shows the effect of Solar cycle

340   24 phase on the Ionization in low latitudes.

341

342   **Figure 6.** Ionization curves from Mitzpe Ramon (Israel), Zaragoza-Barcelona (Spain) and Reading (UK).

343

344 **Figure 7.** Model results of Ion production rate versus altitude from Mitzpe Ramon (Israel), -Barcelona
345 (Spain) and Reading (UK) of the 14 May 2015 Balloon launch.

346

347 **Figure 8.** Observations and modelled ion production rates (top) 14 May 2015 flight and (bottom) 22 Oct
348 2014 flight.

349

350 **Table Captions**

351

352 **Table 1. Summary of balloon launches. (*) Ascent only.**

Launch	Date	Modulation potential [MV]	Flight Duration [s]	Peak Altitude [m]	Pressure [mbar] at peak	Lowest Temperature [°C] recorded	(RP max) cpm @ [km]
1*	6 Oct 2014	677	3149	17542	85.5	-72.3 @ 16.3 km	28.1 cpm at 16.2 km
2*	22 Oct 2014	621	5342	29467	12.6	-74.7 @ 17.2 km	36.1 cpm at 18.5 km
3	14 May 2015	656	6325	28320	15.2	-63.9 @ 20.2 km	31.3 cpm at 16.07 km
4	27 Aug 2015	573	9351	34796	6.1	-74 @ 16.7 km	40.80 cpm at 21.8 km
5*	20 Jun 2016	449	6431	35496	5.4	-74.5 @ 17.5 km	50.87 cpm at 17.1 km
6*	30 Aug 2016	337	7639	28200	16.67	-80.7 @ 17.6 km	47.1 cpm at 19 km

353

354

355

356

357

13

358

Figures:
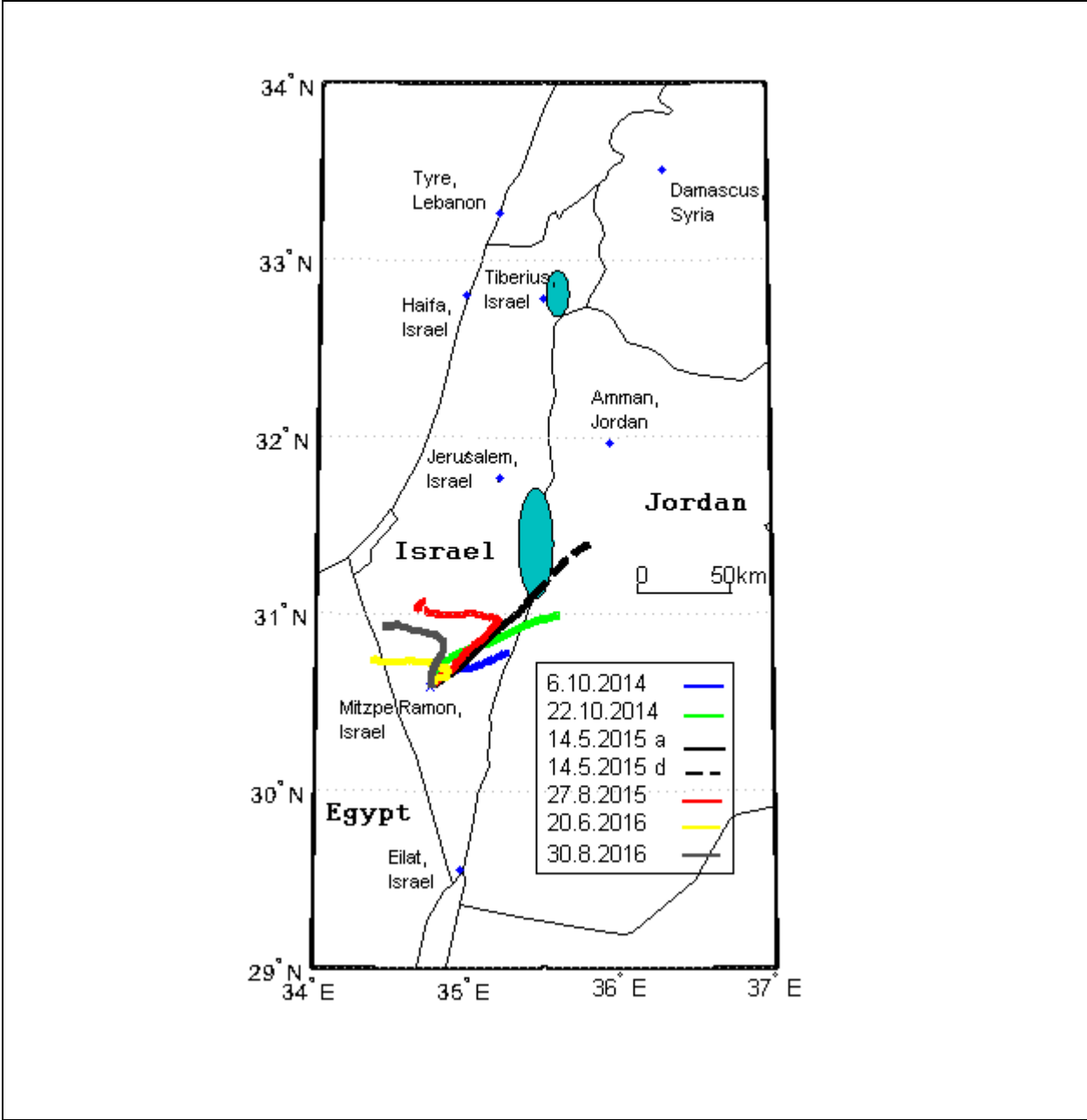
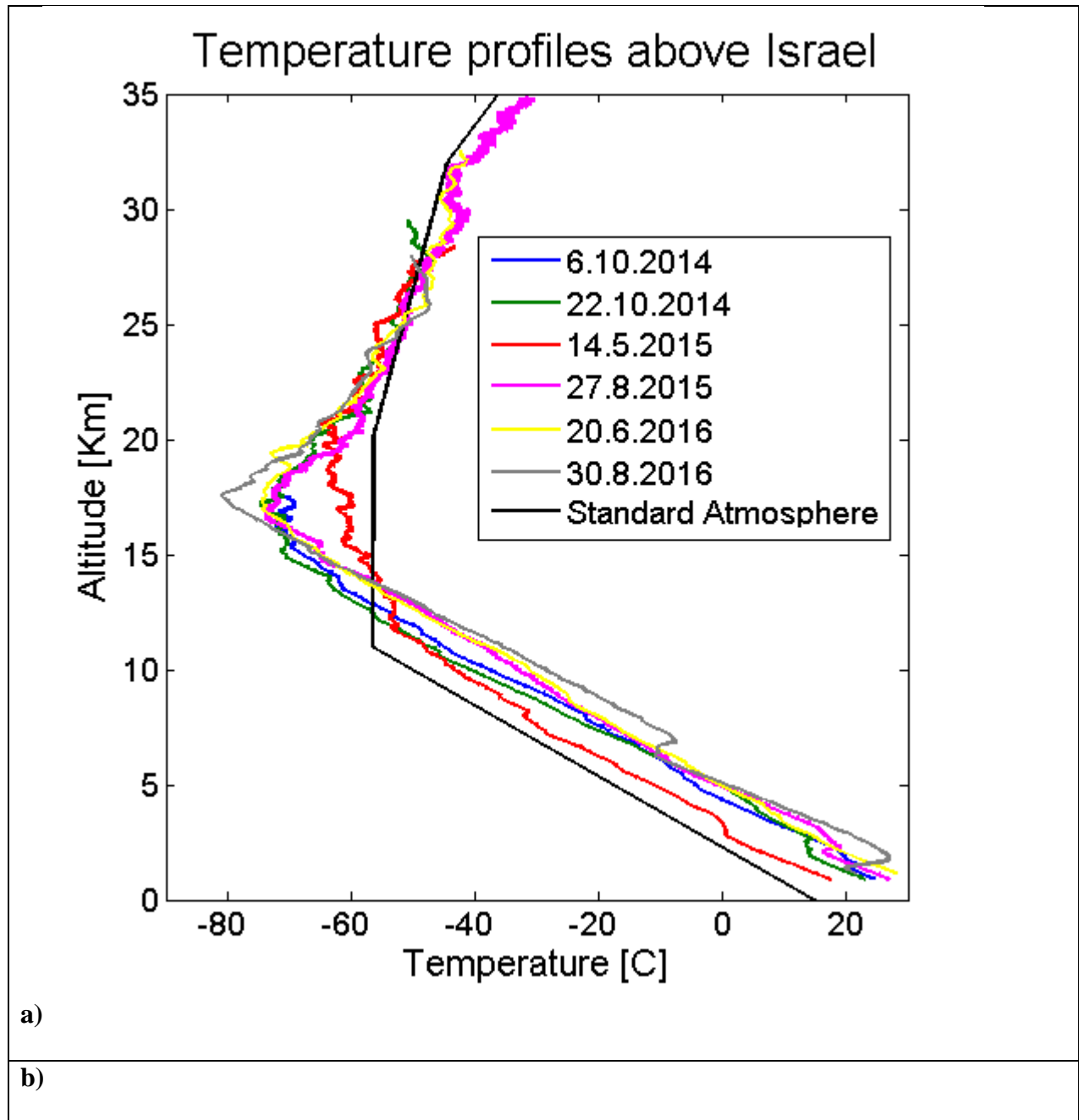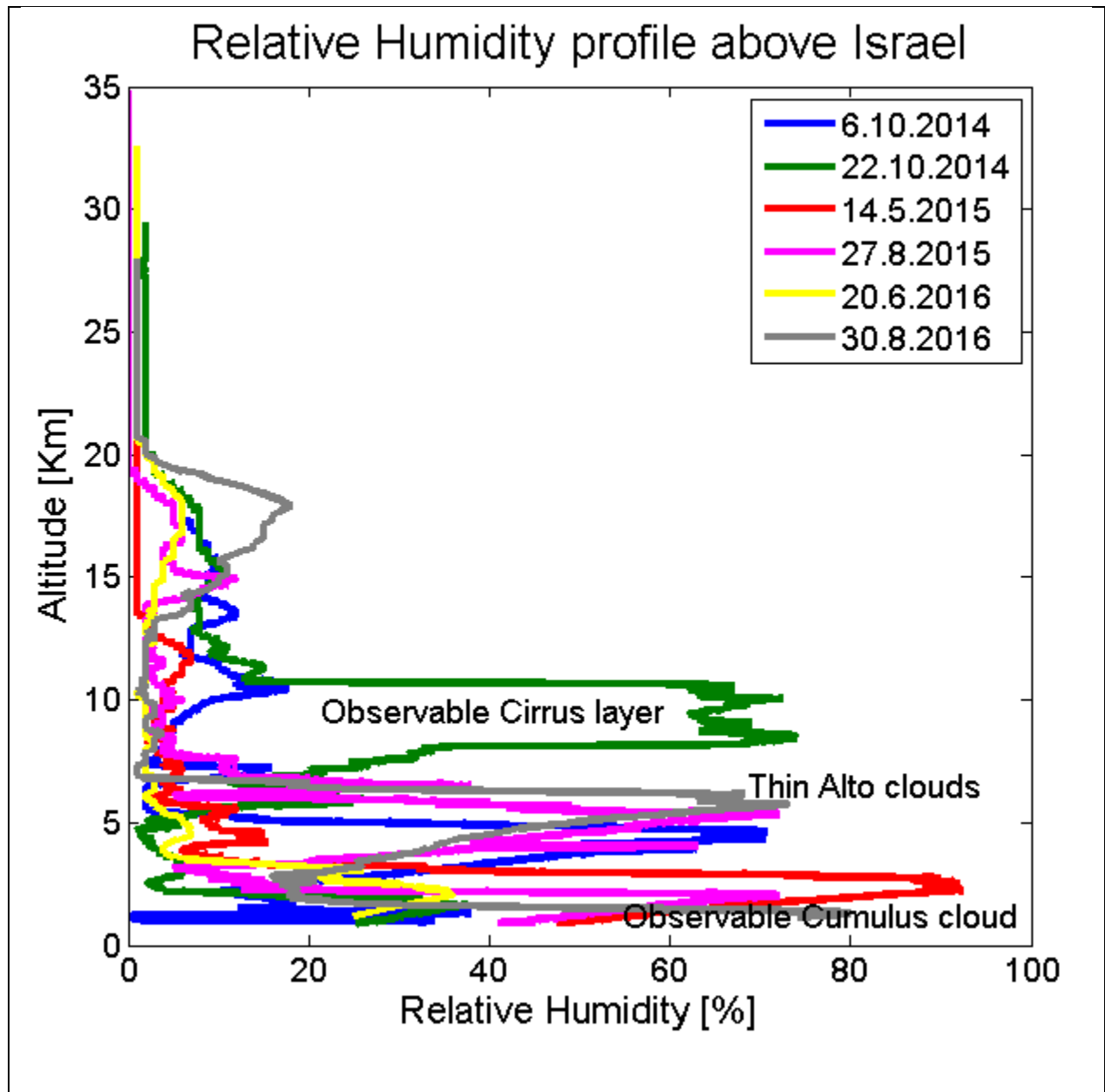**Figure 1:**

361
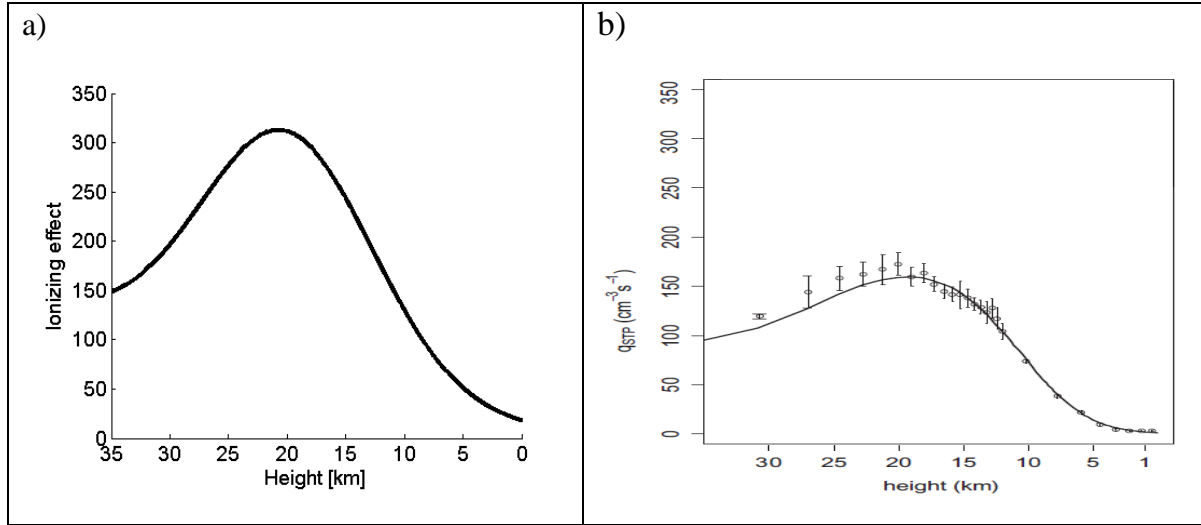
Figure 2:

363

364

365

366

367

Figure 3:

Temperature profiles above Israel

a)

b)

Pressure profile above Israel

Legend:
6.10.2014
22.10.2014
14.5.2015
27.8.2015
14.2.2016
20.6.2016
30.8.2016
Standard Atmosphere

c)

Relative Humidity profile above Israel

Legend:
- 6.10.2014
- 22.10.2014
- 14.5.2015
- 27.8.2015
- 20.6.2016
- 30.8.2016

Observable Cirrus layer

Thin Alto clouds

Observable Cumulus cloud
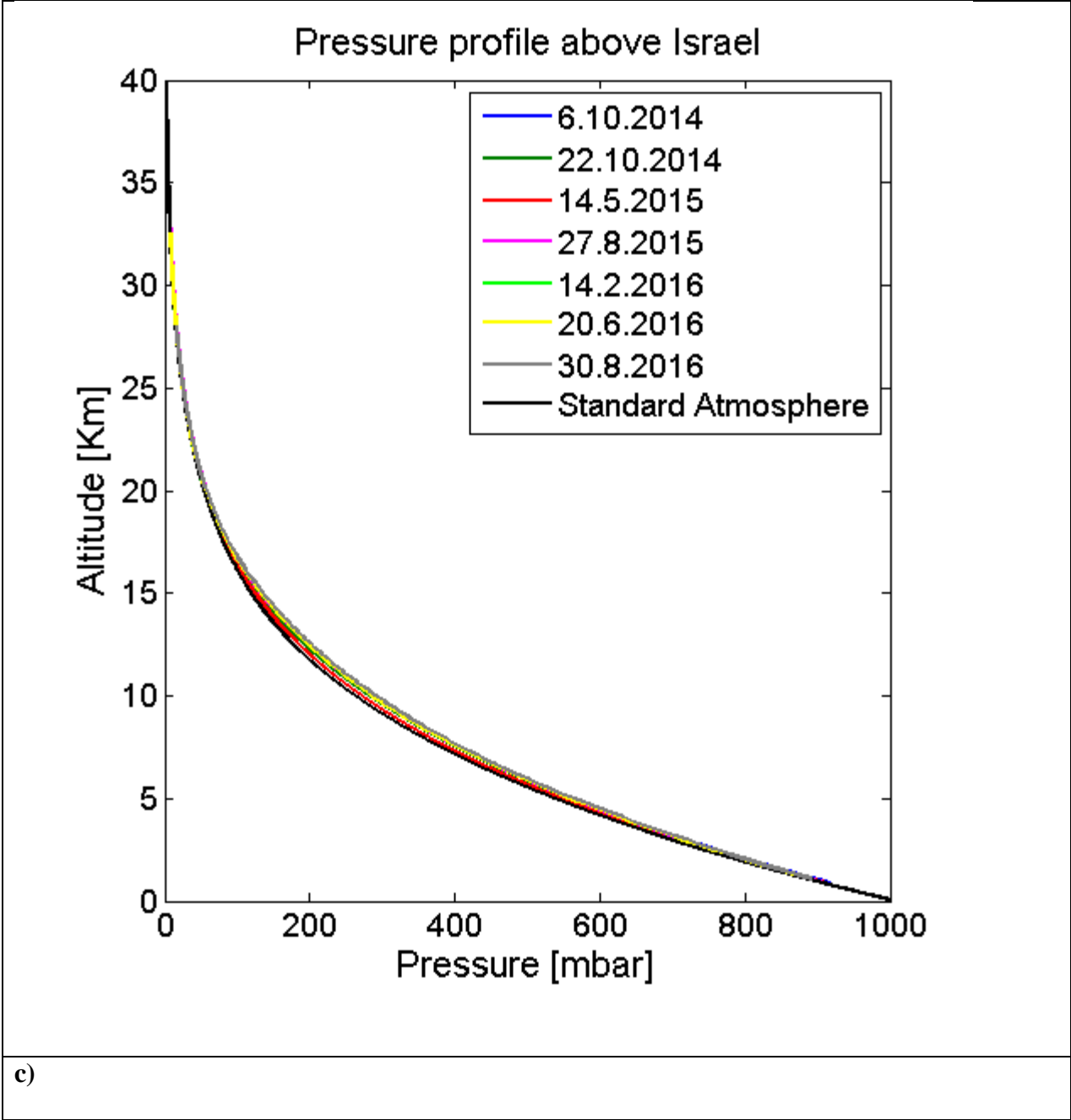
369

370

371

372

373

374

375

376

377 **Figure 4:**

a)

Airborne measurements of Ionisation profile

	6 Oct 2014
	22 Oct 2014
	14 May 2015 Ascent
	14 May 2015 Descent
	27 Aug 2015 Ascent
	27 Aug 2015 Descent
	20 Jun 2016
	30 Aug 2016
	Average Ionisation

b)

Airborne measurements of Ionisation profile
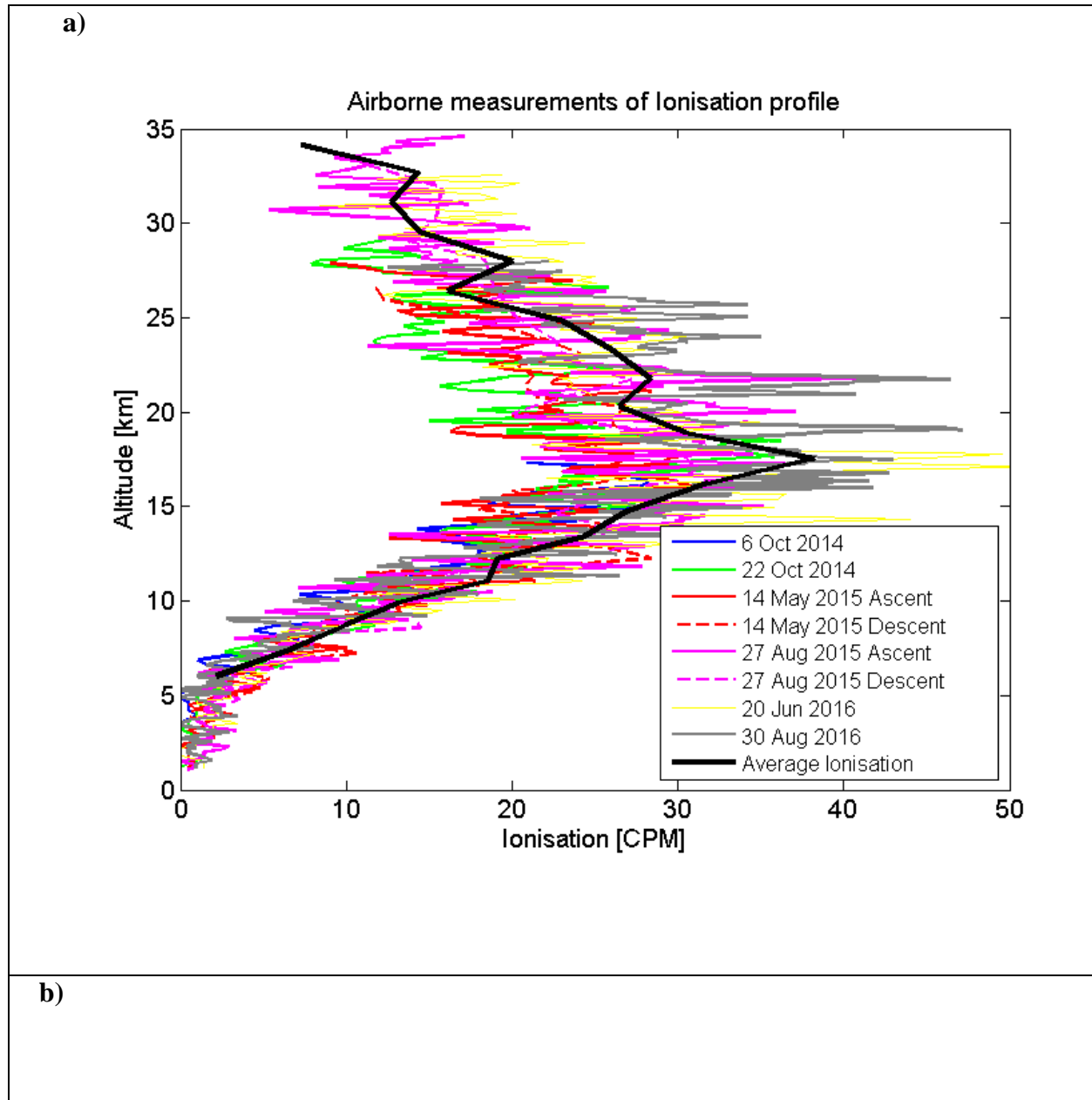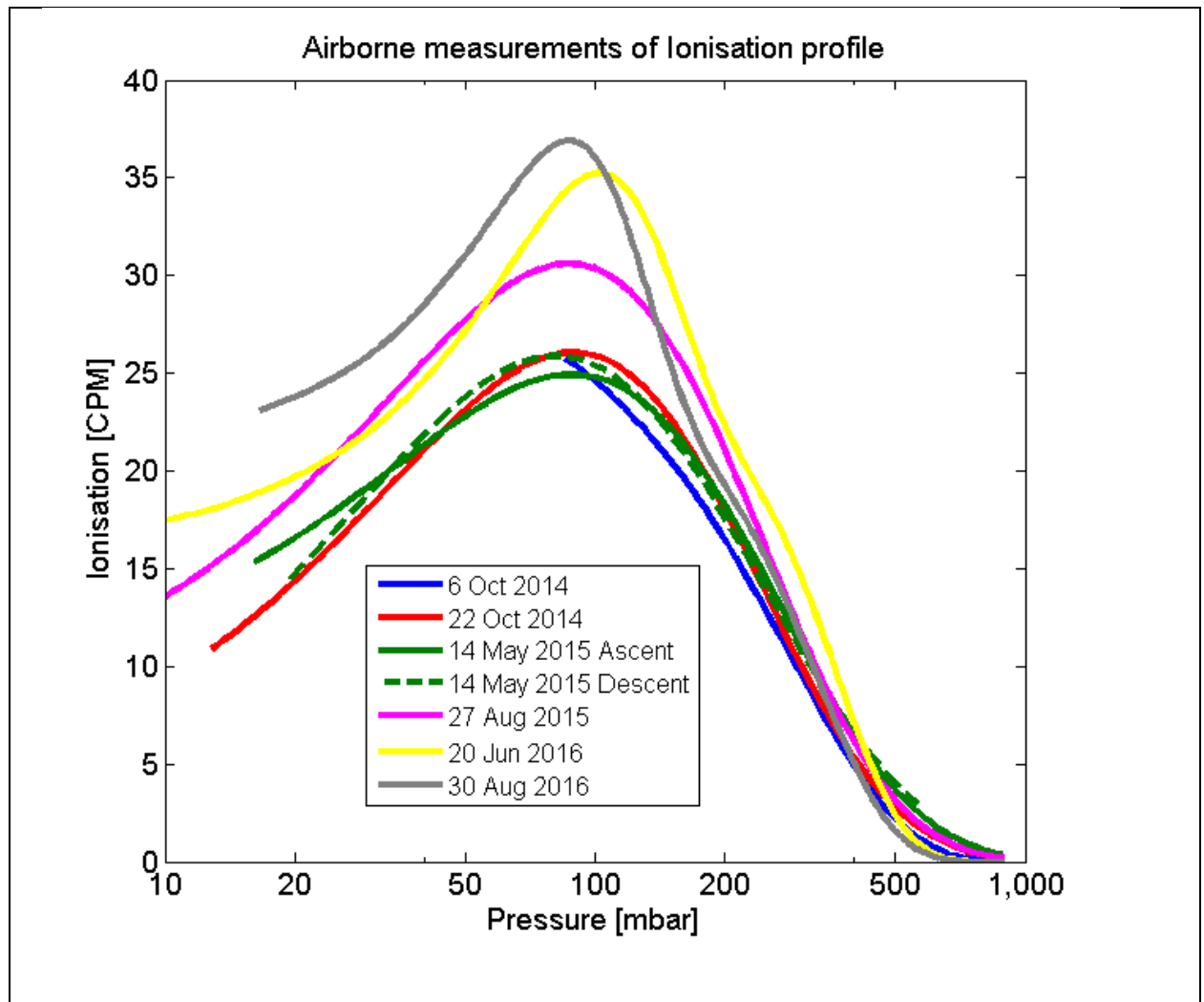
378

379   **Figure 5:**
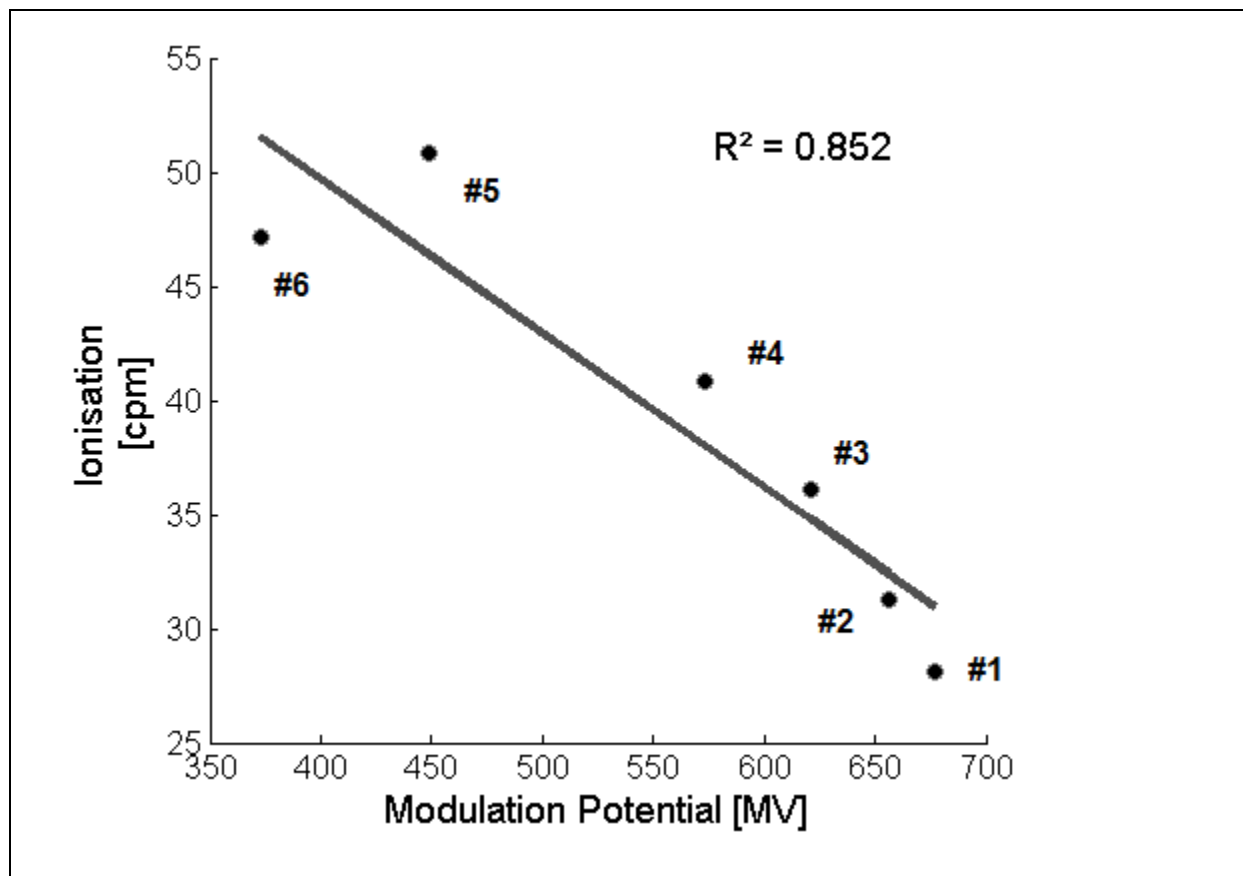
380

381

382

383

384

385

386

387

388

389   **Figure 6:**
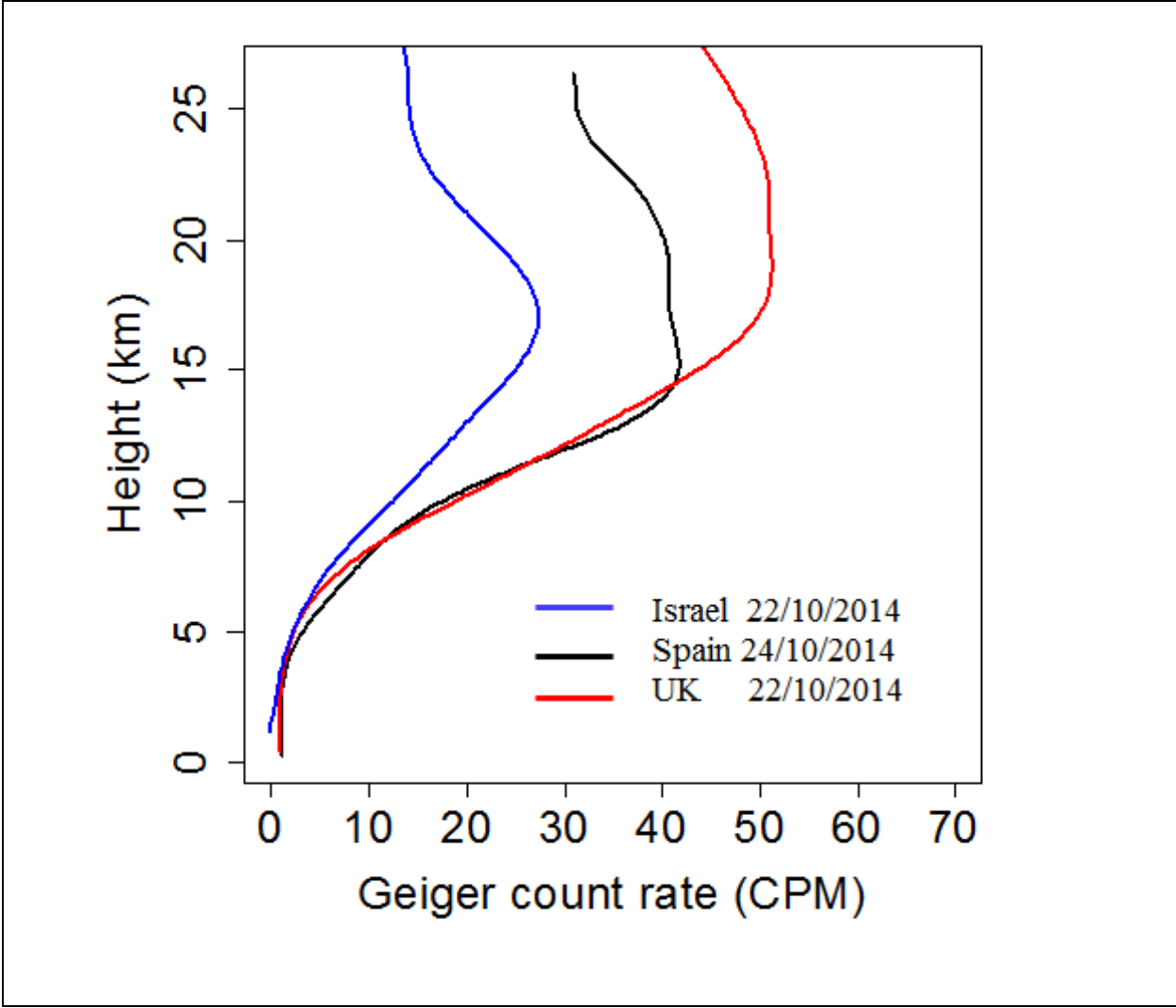
390

391

392

393

394

395

396

397

398

399

400 **Figure 7:**
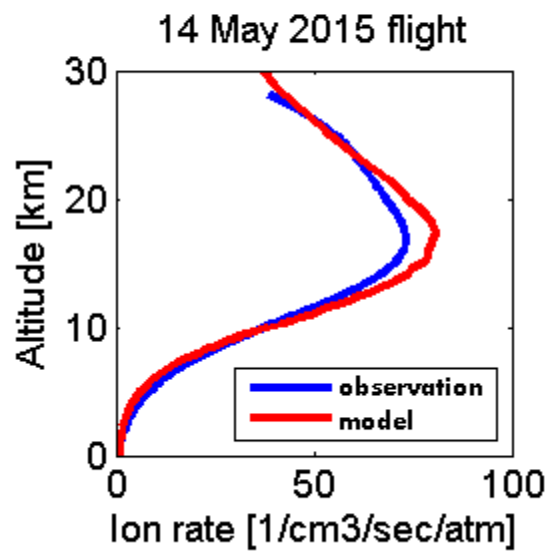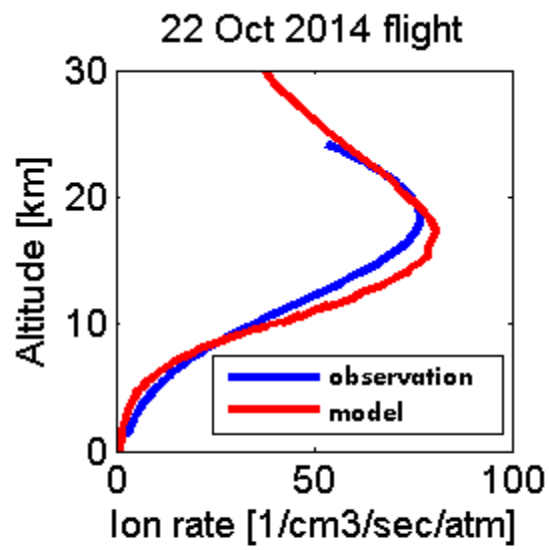

22-24 Oct 2014 model results
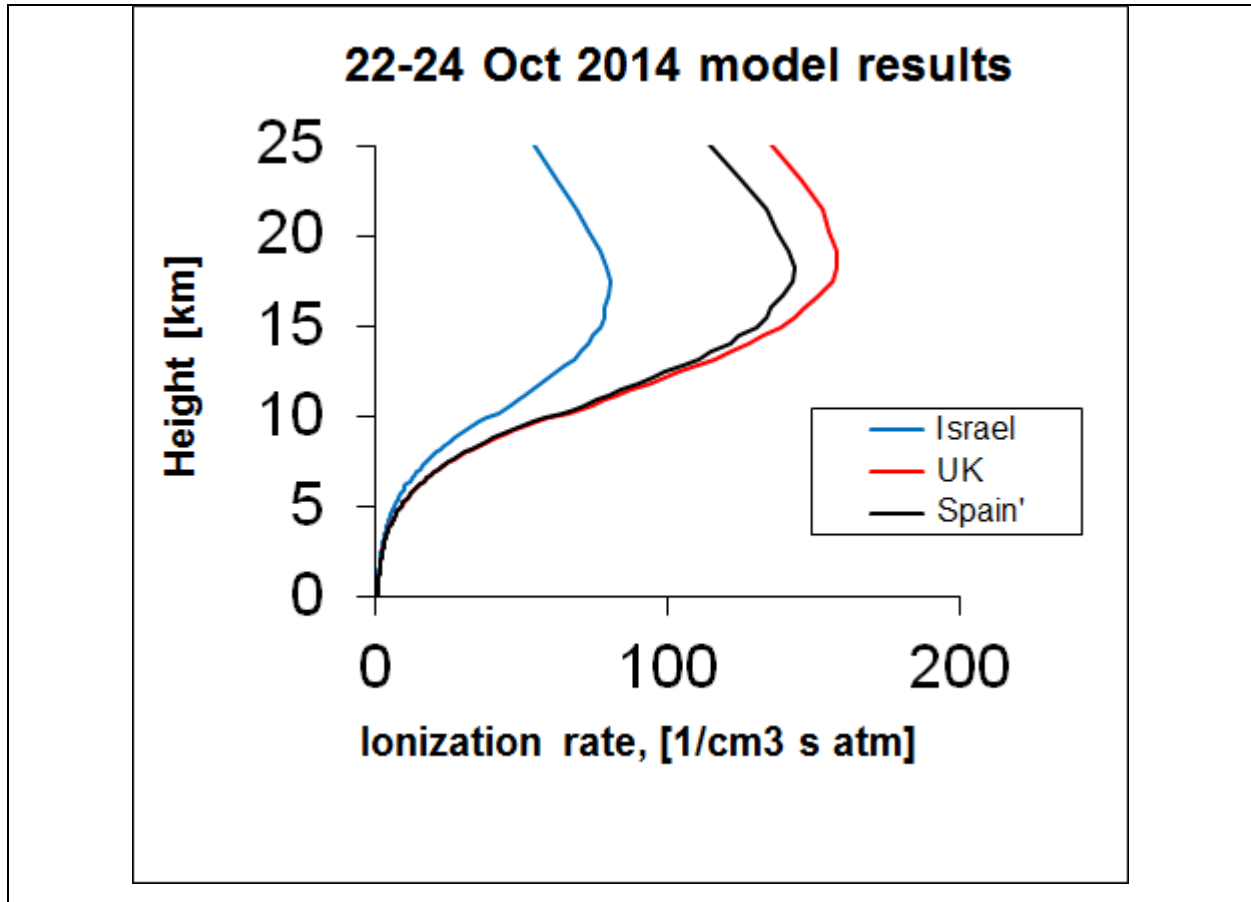
401

402

403

404

405

406

407

408

409

410

411 **Figure 8:**

412

413